Relationship of Cerebrospinal Fluid Markers to ^{11}C-PiB and ^{18}F-FDDNP Binding

Nelleke Tolboom[1,2], Wiesje M. van der Flier[2,3], Maqsood Yaqub[1], Ronald Boellaard[1], Nicolaas A. Verwey[2,4], Marinus A. Blankenstein[4], Albert D. Windhorst[1], Philip Scheltens[2], Adriaan A. Lammertsma[1], and Bart N.M. van Berckel[1]

[1]Departments of Nuclear Medicine and PET Research, VU University Medical Centre, Amsterdam, The Netherlands; [2]Department of Neurology and Alzheimer Centre, VU University Medical Centre, Amsterdam, The Netherlands; [3]Department of Epidemiology and Biostatistics, VU University Medical Centre, Amsterdam, The Netherlands; and [4]Department of Clinical Chemistry, VU University Medical Centre, Amsterdam, The Netherlands

The purpose of this study was to investigate the potential relationships between cerebrospinal fluid (CSF) measurements of β-amyloid-1–42 ($A\beta_{1-42}$) and total tau to ^{11}C-Pittsburgh compound B (^{11}C-PiB) and 2-(1-{6-[(2-^{18}F-fluoroethyl)(methyl)amino]-2-naphthyl}ethylidene) malononitrile (^{18}F-FDDNP) binding as measured using PET. **Methods:** A total of 37 subjects were included, consisting of 15 patients with Alzheimer disease (AD), 12 patients with mild cognitive impairment, and 10 healthy controls. All subjects underwent a lumbar puncture and PET using both ^{11}C-PiB and ^{18}F-FDDNP. For both PET tracers, parametric images of binding potential were generated. Potential associations of CSF levels of $A\beta_{1-42}$ and tau with ^{11}C-PiB and ^{18}F-FDDNP binding were assessed using Pearson correlation coefficients and linear regression analyses. **Results:** For both global ^{11}C-PiB and ^{18}F-FDDNP binding, significant correlations with CSF levels of $A\beta_{1-42}$ ($r = -0.72$ and -0.37, respectively) and tau ($r = 0.58$ and 0.56, respectively) were found across groups (all $P < 0.001$, except $P < 0.05$ for correlation between ^{18}F-FDDNP and $A\beta_{1-42}$). Linear regression analyses showed that, adjusted for regional volume, age, sex, and diagnosis, global ^{11}C-PiB uptake had an inverse association with $A\beta_{1-42}$ CSF levels (standardized $\beta = -0.50$, $P < 0.001$), whereas there was a positive association between global ^{18}F-FDDNP binding and tau CSF levels (standardized $\beta = 0.62$, $P < 0.01$). **Conclusion:** The good agreement between these 2 different types of biomarkers (i.e., CSF and PET) provides converging evidence for their validity. The inverse association between ^{11}C-PiB and CSF tau $A\beta_{1-42}$ confirms that ^{11}C-PiB measures amyloid load in the brain. The positive association between ^{18}F-FDDNP and CSF tau suggests that at least part of the specific signal of ^{18}F-FDDNP in AD patients is due to tangle formation.

Key Words: PET; ^{11}C-PiB, Pittsburgh compound B; ^{18}F-FDDNP; CSF; tau; Alzheimer

J Nucl Med 2009; 50:1464–1470
DOI: 10.2967/jnumed.109.064360

Received Mar. 17, 2009; revision accepted Jun. 4, 2009.
For correspondence or reprints contact: Nelleke Tolboom, Department of Neurology and Alzheimer Centre, VU University Medical Centre, Amsterdam, P.O. Box 7057, 1007 MB, Amsterdam, The Netherlands.
E-mail: n.tolboom@vumc.nl

At present, there are 2 promising methods for the in vivo assessment of the extent of Alzheimer disease (AD) pathology. One is the use of cerebrospinal fluid (CSF) biomarkers of β-amyloid-1–42 ($A\beta_{1-42}$) and tau, the other is the imaging of neuropathology associated with AD using PET and ^{11}C-Pittsburgh compound B (^{11}C-PiB) or 2-(1-{6-[(2-^{18}F-fluoroethyl)(methyl)amino]-2-naphthyl}ethylidene) malononitrile (^{18}F-FDDNP) (*1,2*). Biochemical changes in CSF (decrease of $A\beta_{1-42}$ and increase of tau) are thought to indirectly reflect the presence of AD pathology (*3*). Imaging using either ^{11}C-PiB or ^{18}F-FDDNP is thought to provide a more direct reflection of AD pathology in the brain. ^{11}C-PiB was designed to measure the amount of fibrillar Aβ deposits (*4,5*), which has been confirmed by a postmortem study in AD (*6*). ^{18}F-FDDNP has been reported to label not only amyloid but also neurofibrillary tangles, which colocalized with conventional immunohistochemistry measures (*7,2*) and neuropathologically in an AD patient (*2*). Compared with ^{11}C-PiB, however, limited information is available on in vivo ^{18}F-FDDNP binding in AD patients.

Although it is generally accepted that both types of markers (i.e., CSF and PET) reflect amyloid or tau load, the relationship between these 2 types of biomarkers has not been studied extensively. Only a few studies have investigated the relationship between ^{11}C-PiB and CSF measurements. Studies were performed in groups mainly consisting of healthy controls (*8,9*) or patients with mild cognitive impairment (MCI) (*10,11*) and recently in a group consisting solely of AD patients (*12*). In these studies, an inverse relationship between ^{11}C-PiB and CSF $A\beta_{1-42}$ levels was found but either no (*8*) or only a modest (*10*) relationship between ^{11}C-PiB and CSF tau levels. No studies have been published describing the relationship between ^{18}F-FDDNP binding and CSF biomarker levels.

In our previous study, paired ^{11}C-PiB and ^{18}F-FDDNP studies were performed in AD patients, MCI patients, and healthy controls (*13*). Both tracers were able to distinguish AD patients from healthy controls at a group level, but

specific binding of ^{11}C-PiB in AD patients was substantially higher than that of ^{18}F-FDDNP. The moderate correlation between the global cortical binding of both tracers suggested that they measured related but different aspects of the neuropathology associated with AD. The purpose of the present study was to investigate the potential relationships between CSF measurements of $A\beta_{1-42}$ and tau and PET measurements using ^{11}C-PiB and ^{18}F-FDDNP.

MATERIALS AND METHODS

Subjects

A total of 15 AD patients, 12 patients with amnestic MCI, and 10 healthy controls, for which paired ^{11}C-PiB, ^{18}F-FDDNP, and CSF data were available, were included (*13*). Global and regional ^{11}C-PiB and ^{18}F-FDDNP binding of an overlapping sample has been presented before (*13*). All patients received a standard dementia screening that included medical history, physical and neurologic examinations, laboratory tests, brain MRI, and extensive neuropsychologic testing. Clinical diagnosis was established by consensus in a multidisciplinary team, without knowledge of PET and CSF data. All AD patients met the criteria of the National Institute of Neurological and Communicative Disorders and Stroke–Alzheimer's Disease and Related Disorders Association for probable AD (*14*). MCI patients met Petersen criteria based on subjective and objective cognitive impairment, predominantly affecting memory, in the absence of dementia or significant functional loss (*15*). Control subjects were recruited through advertisements in newspapers and underwent the same diagnostic procedures. Exclusion criteria were a history of major psychiatric or neurologic (other than AD) illness and use of nonsteroidal antiinflammatory drugs, as these have been reported to compete with ^{18}F-FDDNP for binding to Aβ fibrils in vitro and to Aβ plaques ex vivo (*16*). Additional exclusion criteria for controls were subjective memory complaints or clinically significant abnormalities on the MRI scan (as determined by a neuroradiologist). Written informed consent was obtained from all subjects after they had received a complete written and verbal description of the study. The study was approved by the Medical Ethics Review Committee of the VU University Medical Centre, Amsterdam.

PET

PET scans were obtained on an ECAT EXACT HR+ scanner (Siemens/CTI) equipped with a neuroinsert. This scanner enables the acquisition of 63 transaxial planes over a 15.5-cm axial field of view, thus allowing the whole brain to be imaged in a single bed position. The properties of this scanner have been reported previously (*17*). All subjects received a venous cannula for tracer injection. Patient motion was restricted by the use of a head holder and monitored using laser beams. First, a 10-min transmission scan was obtained in 2-dimensional acquisition mode using 3 retractable rotating line sources to correct the subsequent emission scan for photon attenuation. Next, a dynamic emission scan in 3-dimensional acquisition mode was started simultaneously with the intravenous injection of ^{11}C-PiB (354 ± 74 MBq) with a specific activity of 43 ± 25 GBq/μmol using an infusion pump (Med-Rad; Beek), followed by a flush of saline, at a rate of 0.8 mL/s for the first 5 mL and 2.0 mL/s thereafter. Radiolabeled ^{11}C-PiB was synthesized according to a modification (*18*) of the procedure described by Wilson et al. (*19*). The dynamic emission scan consisted of 23 frames, with a progressive increase in frame duration (1 × 15, 3 × 5, 3 × 10, 2 × 30, 3 × 60, 2 × 150, 2 × 300, and 7 × 600 s), for a total duration of 90 min. Finally, after a resting period of at least 1 h to allow for the decay of ^{11}C (i.e., about 2.5 h after the administration of ^{11}C-PiB), the same procedure was repeated but now using an injection of ^{18}F-FDDNP (178 ± 14 MBq) (*20*) with a specific activity of 76 ± 49GBq/μmol.

MRI

All subjects underwent structural MRI using a 1.5-T scanner (Sonata; Siemens Medical Solutions). The scan protocol included coronal T1-weighted 3-dimensional magnetization-prepared rapid-acquisition gradient echo (slice thickness, 1.5 mm; 160 slices; matrix size, 256 × 256; voxel size, 1 × 1 × 1.5 mm; echo time, 3.97 ms; repetition time, 2,700 ms; inversion time, 950 ms; flip angle, 8°), which was used for coregistration and region-of-interest (ROI) definition.

Image Analysis

All PET sinograms were corrected for dead time, tissue attenuation using the transmission scan, decay, scatter, and randoms and were reconstructed using a standard filtered backprojection algorithm and a Hanning filter with a cutoff at 0.5 times the Nyquist frequency. A zoom factor of 2 and a matrix size of 256 × 256 × 63 were used, resulting in a voxel size of 1.2 × 1.2 × 2.4 mm and a spatial resolution of approximately 7 mm in full width at half maximum at the center of the field of view.

MR images were aligned to corresponding PET images using a mutual information algorithm (*21*). Data were further analyzed using PVE lab, a software program that uses a previously validated probability map of 35 delineated ROIs (*22*). No correction for partial-volume effects was applied to the PET data.

ROIs were projected onto ^{11}C-PiB and ^{18}F-FDDNP parametric images of binding potential (BP_{ND}). These parametric images were generated by applying a basis function implementation of the 2-step simplified reference tissue model with cerebellar gray matter as reference tissue (RPM2) (*23*) to the full dynamic 90-min PET data. Recently, RPM2 has been identified as the quantitative method of choice for both tracers (*24,25*). BP_{ND} is a quantitative measure of specific binding, reflecting the concentration of specifically bound tracer relative to the concentration of free and nonspecifically bound tracer in tissue under equilibrium conditions (*26*). All ROIs, including the cerebellum, and their corresponding gray matter volumes were obtained using PVE lab (*22*). For regional analyses, the BP_{ND} of frontal (volume-weighted average of orbital frontal, medial inferior frontal, and superior frontal), parietal, and temporal (volume-weighted average of superior temporal and medial inferior temporal) cortex; medial temporal lobe (MTL) (volume-weighted average of enthorinal cortex and hippocampus); and posterior cingulate was used. In addition, a global cortical ROI was defined, based on the volume-weighted average of these regions. Cerebellar gray matter was chosen as reference tissue because of its (histopathologic) lack of Congo red and thioflavin-S–positive plaques (*27,28*).

CSF

CSF was obtained by lumbar puncture (LP) of the L3/L4 or L4/L5 intervertebral space, using a 25-gauge needle, and collected in 10-mL polypropylene tubes. Within 2 h, CSF samples were centrifuged at 1,800*g* for 10 min at 4°C. A small amount of CSF was used for routine analysis, including total cells (leukocytes and erythrocytes), total protein, and glucose. CSF was separated into aliquots in polypropylene tubes (0.5 or 1 mL) and

stored at −80°C until further analysis. CSF $A\beta_{1-42}$ and tau were measured with Innotest (Innogenetics) sandwich enzyme-linked immunosorbent assay as described previously (*29*). As the manufacturer does not supply control data, performance of the assays was monitored using pools of surplus CSF specimens. In the study period, multiple specimens with various concentrations, which were included in 7–18 runs, were used for this purpose. The mean coefficients of variation (±SD) obtained were 11.3% ± 4.9% for $A\beta_{1-42}$ and 9.3% ± 1.5% for tau. Median time from LP to PET was 3 mo (interquartile range, 6 months). Five subjects (2 AD patients, 1 MCI patient, and 2 controls) received their LP more than 12 months apart from (before) the PET scan. After exclusion of these subjects, median time from LP to PET was 2.5 months.

Statistical Analysis

Data are presented as mean ± SD, unless otherwise stated. As CSF biomarker levels were not normally distributed, data were log-transformed. Frequency distributions for sex were compared with χ^2 tests. For continuous measures, differences between groups were assessed using ANOVA with post hoc least-significant-difference tests and age as covariate.

For the assessment of relationships between CSF and BP_{ND} data, first Pearson correlations were calculated across the entire group. Next, linear regression analyses were performed to adjust for potential confounders using CSF biomarkers as independent and global and regional BP_{ND} as dependent variables. Separate analyses were performed for ^{11}C-PiB and ^{18}F-FDDNP. In the first model, the relationship of each CSF biomarker with both PET tracers was adjusted for gray matter ROI volume. In the second model, analyses were additionally adjusted for age, sex, and diagnosis (using dummy variables). In the third model, CSF biomarkers were entered simultaneously, together with the same covariates. This analysis was repeated after exclusion of the 5 subjects with long intervals between LP and PET. Standardized βs are reported to allow comparison of effect sizes. A P value below 0.05 was considered significant.

RESULTS

Demographic and clinical data by patient group are presented in Table 1. The 3 groups were similar with respect to sex. AD patients tended to be younger than MCI patients and controls. AD patients had lower Mini-Mental State Examination scores than control subjects and MCI patients (both $P \leq 0.001$). Group differences were found for CSF levels of $A\beta_{1-42}$ and tau ($P \leq 0.001$). In addition, groups differed with respect to global cortical ^{11}C-PiB BP_{ND} ($P \leq 0.001$). A trend was seen for global cortical ^{18}F-FDDNP BP_{ND} ($P < 0.10$). Figure 1 shows parametric ^{11}C-PiB and ^{18}F-FDDNP BP_{ND} images of a typical AD patient and a healthy control.

Table 2 lists Pearson correlations between $A\beta_{1-42}$ and tau levels in CSF and global and regional tracer BP_{ND} across all subjects. Lower $A\beta_{1-42}$ and higher tau levels were associated with higher global ^{11}C-PiB binding (Fig. 2). This was due to higher binding in all cortical regions investigated for $A\beta_{1-42}$ and in all, except the MTL, for tau. Furthermore, lower $A\beta_{1-42}$ and higher tau levels were associated with higher global ^{18}F-FDDNP binding (Fig. 3). In this case, lower CSF $A\beta_{1-42}$ was associated with higher uptake in frontal and parietal cortex, but there were no correlations with other brain regions investigated. Higher CSF levels of tau were associated with higher uptake in all regions, except the MTL.

TABLE 1. Demographic and Clinical Characteristics of 3 Diagnostic Groups

Characteristic	Control	MCI	AD
n	10	12	15
Age (y)*	70 ± 6	68 ± 9	63 ± 7
Sex (F/M)	3/7	2/10	6/9
MMSE†	29 ± 1	28 ± 2	24 ± 2‡,§
$A\beta_{1-42}$ (pg/mL)†	886 ± 244	623 ± 165§	507 ± 78§
Tau (pg/mL)†	264 ± 104	431 ± 269	752 ± 371§,‖
^{11}C-PiB BP_{ND}			
Global†	0.18 ± 0.30	0.33 ± 0.37	0.86 ± 0.12‡,§
Frontal	0.22 ± 0.37	0.37 ± 0.42	0.93 ± 0.11‡,§
Medial temporal	0.08 ± 0.08	0.07 ± 0.06	0.15 ± 0.09‖,¶
Temporal	0.16 ± 0.27	0.31 ± 0.34	0.79 ± 0.11‡,§
Posterior cingulate	0.17 ± 0.22	0.37 ± 0.38	0.84 ± 0.41‡,§
Parietal	0.17 ± 0.30	0.34 ± 0.21	0.96 ± 0.20‡,§
^{18}F-FDDNP BP_{ND}			
Global*	0.06 ± 0.03	0.08 ± 0.05	0.09 ± 0.02
Frontal*	0.05 ± 0.04	0.09 ± 0.06	0.09 ± 0.02
Medial temporal	0.12 ± 0.04	0.13 ± 0.05	0.14 ± 0.05
Temporal	0.07 ± 0.03	0.10 ± 0.05	0.10 ± 0.03
Posterior cingulate	0.04 ± 0.01	0.07 ± 0.02	0.06 ± 0.01
Parietal	0.02 ± 0.04	0.04 ± 0.04	0.06 ± 0.03

ANOVA with age as covariate:
*$P < 0.10$.
†$P \leq 0.001$.
Post hoc least-significant difference tests:
‡$P \leq 0.001$, compared with MCI.
§$P \leq 0.001$, compared with controls.
‖$P < 0.05$, compared with MCI.
¶$P < 0.05$, compared with controls.
Data are mean ± SD, where appropriate. Note that raw values are shown for CSF biomarkers (pg/mL) but that log-transformed values were used for statistical analysis.
MMSE = Mini-Mental State Examination.

Next, linear regression analyses were performed to adjust for potential confounders. After adjustment for gray matter ROI volume (model 1), associations were observed between both CSF markers (i.e., low CSF $A\beta_{1-42}$ and high CSF tau) and increased global and regional ^{11}C-PiB binding (Table 3). For ^{18}F-FDDNP binding, associations were found between low CSF $A\beta_{1-42}$ and increased global, frontal, and parietal binding, with a trend for temporal binding. In addition, associations were found between high CSF tau and increased ^{18}F-FDDNP binding in all regions except for the MTL, where this association displayed only a trend (standardized $\beta = 0.34$, $P < 0.10$).

After additionally adjusting for age, sex, and diagnosis (model 2), an association was observed between CSF $A\beta_{1-42}$

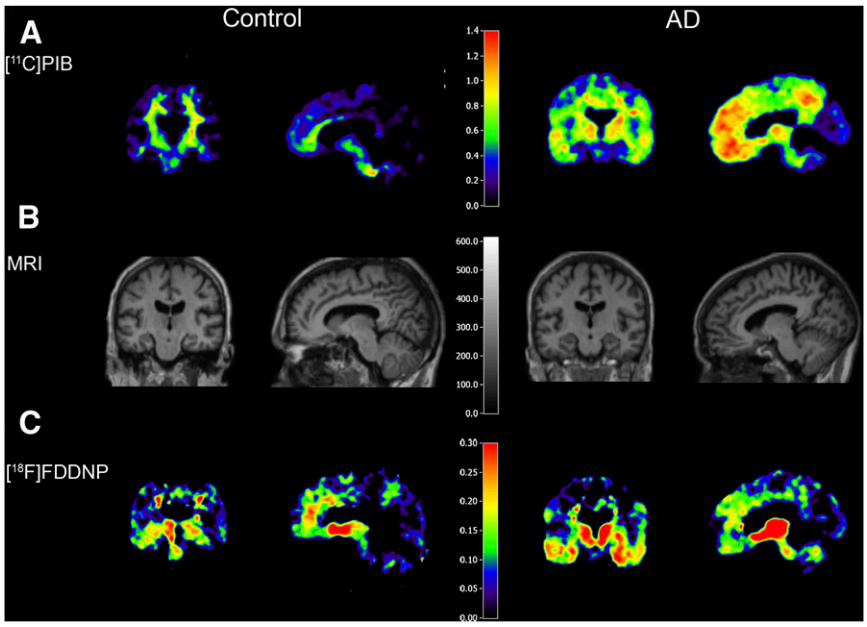

FIGURE 1. Examples of parametric coronal (left column) and sagittal (right column) ^{11}C-PiB and ^{18}F-FDDNP BP_{ND} images in control subject and AD patient with their coregistered MR image. ^{11}C-PiB and ^{18}F-FDDNP scans were obtained in same subjects. Corresponding CSF values for AD patient (60 y) were $A\beta_{1-42}$, 504 pg/mL, and tau, 837 pg/mL. For the healthy control (61 y), CSF levels were $A\beta_{1-42}$, 1,123 pg/mL, and tau, 245 pg/mL.

and global, frontal, temporal, and posterior cingulate ^{11}C-PiB binding, but there was no such association between CSF tau and global or regional ^{11}C-PiB binding. For ^{18}F-FDDNP binding, the opposite pattern was observed (i.e., a positive association with CSF levels of tau but no association with CSF levels of $A\beta_{1-42}$). For the MTL, no associations were found after correcting for gray matter ROI volume, age, sex, and diagnosis. Nevertheless, the effect size of the association between CSF tau and ^{18}F-FDDNP binding in this region remained comparable (standardized $\beta = 0.33$). Results were essentially the same in the third model, in which both CSF biomarkers were entered simultaneously (data not shown). Finally, these analyses were repeated after exclusion of the 5 subjects with intervals between LP and PET of more than 12 mo. Results remained unaltered for associations with ^{11}C-PiB binding (model 2, global binding; CSF $A\beta_{1-42}$: standardized $\beta = -0.50$, $P < 0.01$; CSF tau: standardized $\beta = 0.19$, $P = 0.29$). For ^{18}F-FDDNP, associations with both CSF $A\beta_{1-42}$ and tau became even stronger (model 2, global binding; CSF tau standardized $\beta = 0.70$, $P < 0.01$; CSF $A\beta_{1-42}$: standardized $\beta = -0.42$, $P = 0.09$). Again, results were essentially the same in the third model, in which both CSF biomarkers were entered simultaneously (data not shown).

TABLE 2. Pearson Correlation Coefficients Between CSF Biomarkers and Tracer BP_{ND}

	CSF biomarker (pg/mL)			
	BP_{ND} ^{11}C-PiB		BP_{ND} ^{18}F-FDDNP	
Brain region	$A\beta_{1-42}$	Tau	$A\beta_{1-42}$	Tau
Global	−0.72*	0.58*	−0.37†	0.56*
Frontal	−0.74*	0.58*	−0.37†	0.56*
Medial temporal	−0.36†	0.26	−0.13	0.25
Temporal	−0.71*	0.59*	−0.26	0.45†
Posterior cingulated	−0.69*	0.53†	−0.12	0.33†
Parietal	−0.68*	0.56*	−0.39†	0.48†

*$P \leq 0.001$.
†$P < 0.05$.

DISCUSSION

In the present study, relationships between 2 CSF biomarkers ($A\beta_{1-42}$ and tau) and uptake of 2 PET amyloid tracers (^{11}C-PiB and ^{18}F-FDDNP) were investigated. Adjusted for ROI volume, age, sex, and diagnosis, increased global ^{11}C-PiB binding was specifically related to low CSF levels of $A\beta_{1-42}$. In contrast, increased global ^{18}F-FDDNP binding was associated with high CSF levels of tau. These results add to the converging evidence that both PET tracers measure different elements of the neuropathology underlying AD.

These results confirm and extend those of previous studies in which an inverse (*12,8–10*) relationship between CSF $A\beta_{1-42}$ and ^{11}C-PiB and no (*8*) or only a modest (*10*) relationship between CSF tau and ^{11}C-PiB were demonstrated. Those earlier studies, however, were performed in groups consisting mainly of healthy controls (*8,9*), MCI patients (*10*), or AD patients (*12*). In the present study, this relationship was extended to the entire spectrum of cognitive decline, providing further support for the notion that ^{11}C-PiB measures amyloid load in the brain.

No associations between ^{18}F-FDDNP binding and CSF data have been reported. Although it has been previously reported that ^{18}F-FDDNP binds with high affinity to both amyloid plaques and neurofibrillary tangles in vitro (*7*), a considerably lower sensitivity for binding to amyloid containing structures has been reported recently (*30*). At

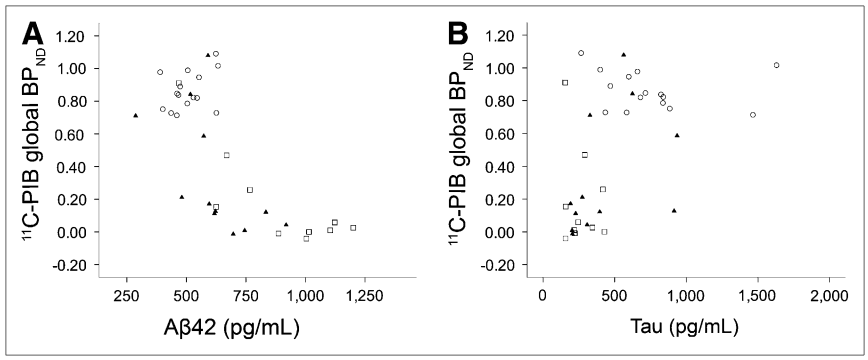

FIGURE 2. Scatter plots of ^{11}C-PiB binding (global BP_{ND}) against CSF levels of $A\beta_{1-42}$ (A) and tau (B). ○ are patients with AD, ▲ are patients with MCI, and □ are healthy controls. CSF values are shown as measured, whereas statistical analyses were performed on log-transformed values. Lower CSF levels of $A\beta_{1-42}$ (A: $r = -0.72$, $P < 0.001$) and higher tau levels (B: $r = 0.58$, $P < 0.001$) were associated with higher global ^{11}C-PiB binding.

present, it is still not clear what the specific signal in AD represents in vivo. In the present data, a positive association between ^{18}F-FDDNP and CSF tau and, after exclusion of 5 subjects with long intervals between PET and CSF sampling, a moderate inverse association with CSF levels of $A\beta_{1-42}$ were observed. These results suggest that increased binding of ^{18}F-FDDNP in AD patients may indeed be due to tangle formation and, to some extent, plaques. This is in line with a previous study (*7*) showing ^{18}F-FDDNP autopsy tissue staining to colocalize with conventional histochemistry measures of tangles and plaques.

After exclusion of the 5 subjects with long intervals between PET and LP, a moderate inverse association was found between ^{18}F-FDDNP binding and CSF levels of $A\beta_{1-42}$, which was not present beforehand. Previously, it was shown that in the case of repeated LP, CSF biomarkers hardly change over time (*29*). Therefore, these results are unlikely to be caused by changes in CSF. For ^{18}F-FDDNP, an increase in binding over time has been described in subjects with clinical evidence of disease progression (*2*). Therefore, changes in the substrate for ^{18}F-FDDNP binding are more likely to have contributed to these results. Furthermore, exclusion of relative outliers could also have contributed to the stronger association.

In general, for both tracers associations between regional tracer binding and CSF biomarkers were similar to those for global binding, except for the MTL, in which no associations were found. This finding is remarkable for ^{18}F-FDDNP, because the MTL displayed the highest ^{18}F-FDDNP binding values for all 3 diagnostic groups. The lack of associations in this region may be due to technical reasons. This region, being the volume-weighted average of the entorhinal cortex and hippocampus, was relatively small, making it sensitive to noise. Furthermore, because the MTL atrophy is commonly seen in AD (*31*), differences in MTL volumes between diagnostic groups may lead to partial-volume effects and thus underestimation of the signal in AD patients. This potentially causes reduced variability in the MTL BP_{ND} between diagnostic groups and consequently a lack of association with CSF biomarkers. When linear regression analyses were performed with adjustment for gray matter ROI volume, a trend was found for high CSF levels of tau to be associated with increased ^{18}F-FDDNP binding in the MTL. After additional adjustment for age, sex, and diagnosis, this trend disappeared—although the effect size remained strong—suggesting that indeed partial-volume effects in the MTL have at least partly underestimated tracer binding in this region. However, PET data were not corrected for partial-volume effects. The choice was made not to correct for partial voluming, as potential overcorrection may lead to an artificially high signal. This approach ascertains that any observed increase in binding is real, which is a deliberate conservative approach. But more important, the current status of partial-volume correction (PVC) in amyloid imaging is not clear. For ^{11}C-PiB studies, several PVC methods have been used, most commonly a method developed by Meltzer et al. (*32*) and an algorithm implemented in the PMOD software package (PMOD Technologies Ltd.). These methods are based on T1-weighted structural

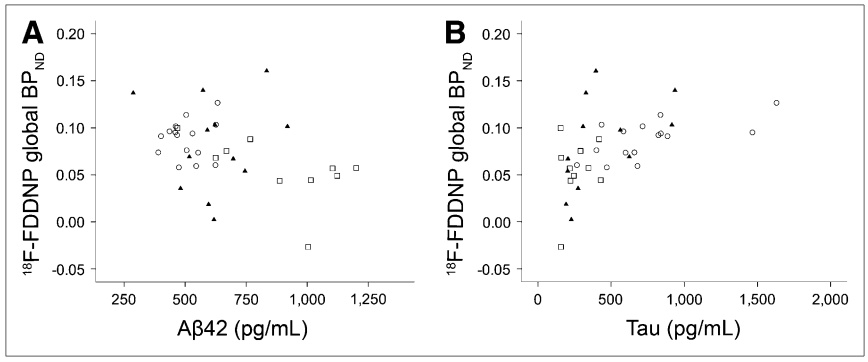

FIGURE 3. Scatter plots of ^{18}F-FDDNP binding (global BP_{ND}) against CSF levels of $A\beta_{1-42}$ (A) and tau (B). ○ are patients with AD, ▲ are patients with MCI, and □ are healthy controls. CSF values are shown as measured, whereas statistical analyses were performed on log-transformed values. Lower CSF levels of $A\beta_{1-42}$ (A: $r = -0.37$, $P < 0.05$) and higher tau levels (B: $r = 0.56$, $P < 0.001$) were associated with higher global ^{18}F-FDDNP binding.

TABLE 3. Linear Regression Analysis Between CSF Biomarkers and Tracer BP_{ND}

	CSF biomarker (pg/mL)			
	Model 1		Model 2	
Brain region	$A\beta_{1-42}$	Tau	$A\beta_{1-42}$	Tau
^{11}C-PiB BP_{ND}				
Global ^{11}C-PiB	−0.72*	0.59*	−0.50*	0.17
Frontal	−0.75*	0.60*	−0.56*	0.18
Medial temporal	−0.42†	0.37†	−0.15	0.03
Temporal	−0.69*	0.57*	−0.46*	0.17
Posterior cingulate	−0.69*	0.52*	−0.47†	0.12
Parietal	−0.67*	0.57*	−0.43†	0.14
^{18}F-FDDNP BP_{ND}				
Global ^{18}F-FDDNP	−0.36†	0.59*	−0.26	0.62†
Frontal	−0.36†	0.56*	−0.27	0.62†
Medial temporal	−0.16	0.34‡	−0.07	0.33
Temporal	−0.29‡	0.56*	−0.12	0.50†
Posterior cingulate	−0.12	0.33†	−0.03	0.46†
Parietal	−0.36†	0.49†	−0.33	0.44†

*$P \leq 0.001$.
†$P < 0.05$.
‡$P < 0.10$.
Linear regression analyses were performed to adjust for potential confounders. Model 1, adjusted for ROI volume; model 2, adjusted for ROI volume, age, sex, and diagnosis (using dummy variables). Values are given as standardized βs.

MRI scans. However, a study performed by our group (*33*) showed that accuracy of MRI-based PVC depends greatly on MRI scanner type, scanning sequence, and gray or white matter segmentation algorithm. The results of that study indicate that the accuracy of PVC should be further evaluated before it can be used in patient studies.

CONCLUSION

The main strength of the present study is its unique design: CSF sampling and PET with both ligands in the same subjects along the spectrum of cognitive decline. This design enabled a direct assessment of the relationship between 2 types of biomarkers, both aimed at identifying underlying AD pathology. The inverse association between ^{11}C-PiB and CSF tau $A\beta_{1-42}$ confirms that ^{11}C-PiB measures amyloid load in the brain. The positive association between ^{18}F-FDDNP and CSF tau suggests that at least part of the specific signal of ^{18}F-FDDNP in AD patients is due to tangle formation. Further research in tauopathies other than AD will be valuable in gaining more insight in the validity of ^{18}F-FDDNP for in vivo imaging of tau pathology. In addition, longitudinal studies are needed to investigate possible increases in ^{18}F-FDDNP binding over time.

ACKNOWLEDGMENTS

We thank Anke A. Dijkstra for help with the data analysis, the PET radiochemistry and technology staff of the Division of Nuclear Medicine and PET Research for tracer production and acquisition of PET data, and the technology staff of the Department of Radiology for acquisition of the MRI data. This work was financially supported by the Internationale Stichting Alzheimer Onderzoek (ISAO; grant 05512) and the American Health Assistance Foundation (AHAF; grant A2005-026). The clinical database structure was developed with funding from Stichting Dioraphte.

REFERENCES

1. Klunk WE, Engler H, Nordberg A, et al. Imaging brain amyloid in Alzheimer's disease with Pittsburgh Compound-B. *Ann Neurol.* 2004;55:306–319.
2. Small GW, Kepe V, Ercoli LM, et al. PET of brain amyloid and tau in mild cognitive impairment. *N Engl J Med.* 2006;355:2652–2663.
3. Blennow K, Hampel H. CSF markers for incipient Alzheimer's disease. *Lancet Neurol.* 2003;2:605–613.
4. Klunk WE, Lopresti BJ, Ikonomovic MD, et al. Binding of the positron emission tomography tracer Pittsburgh compound-B reflects the amount of amyloid-β in Alzheimer's disease brain but not in transgenic mouse brain. *J Neurosci.* 2005;25:10598–10606.
5. Klunk WE, Wang Y, Huang GF, et al. The binding of 2-(4′-methylaminophenyl)benzothiazole to postmortem brain homogenates is dominated by the amyloid component. *J Neurosci.* 2003;23:2086–2092.
6. Ikonomovic MD, Klunk WE, Abrahamson EE, et al. Post-mortem correlates of in vivo PiB-PET amyloid imaging in a typical case of Alzheimer's disease. *Brain.* 2008;131:1630–1645.
7. Agdeppa ED, Kepe V, Liu J, et al. Binding characteristics of radiofluorinated 6-dialkylamino-2-naphthylethylidene derivatives as positron emission tomography imaging probes for β-amyloid plaques in Alzheimer's disease. *J Neurosci.* 2001;21:RC189.
8. Fagan AM, Mintun MA, Mach RH, et al. Inverse relation between in vivo amyloid imaging load and cerebrospinal fluid $A\beta_{42}$ in humans. *Ann Neurol.* 2006;59:512–519.
9. Fagan AM, Roe CM, Xiong C, Mintun MA, Morris JC, Holtzman DM. Cerebrospinal fluid tau/β-$amyloid_{42}$ ratio as a prediction of cognitive decline in nondemented older adults. *Arch Neurol.* 2007;64:343–349.
10. Forsberg A, Engler H, Almkvist O, et al. PET imaging of amyloid deposition in patients with mild cognitive impairment. *Neurobiol Aging.* 2008;29:1456–1465.
11. Koivunen J, Pirttila T, Kemppainen N, et al. PET amyloid ligand [^{11}C]PIB uptake and cerebrospinal fluid β-amyloid in mild cognitive impairment. *Dement Geriatr Cogn Disord.* 2008;26:378–383.
12. Grimmer T, Riemenschneider M, Forstl H, et al. Beta amyloid in Alzheimer's disease: increased deposition in brain is reflected in reduced concentration in cerebrospinal fluid. *Biol Psychiatry.* 2009;65:927–934.
13. Tolboom N, Yaqub M, van der Flier WM, et al. Detection of Alzheimer pathology in vivo using both ^{11}C-PIB and ^{18}F-FDDNP positron emission tomography. *J Nucl Med.* 2009;50:191–197.
14. McKhann G, Drachman D, Folstein M, Katzman R, Price D, Stadlan EM. Clinical diagnosis of Alzheimer's disease: report of the NINCDS-ADRDA Work Group under the auspices of Department of Health and Human Services Task Force on Alzheimer's Disease. *Neurology.* 1984;34:939–944.
15. Petersen RC, Smith GE, Waring SC, Ivnik RJ, Tangalos EG, Kokmen E. Mild cognitive impairment: clinical characterization and outcome. *Arch Neurol.* 1999;56:303–308.
16. Agdeppa ED, Kepe V, Petri A, et al. In vitro detection of (*S*)-naproxen and ibuprofen binding to plaques in the Alzheimer's brain using the positron emission tomography molecular imaging probe 2-(1-[6-[(2-[^{18}F]fluoroethyl)(methyl)amino]-2-naphthyl]ethylidene)malono nitrile. *Neuroscience.* 2003;117:723–730.
17. Brix G, Zaers J, Adam LE, et al. Performance evaluation of a whole-body PET scanner using the NEMA protocol. National Electrical Manufacturers Association. *J Nucl Med.* 1997;38:1614–1623.
18. Tolboom N, Yaqub M, Boellaard R, et al. Test-retest variability of quantitative [^{11}C]PIB studies in Alzheimer's disease. *Eur J Nucl Med.* April 29, 2009 [Epub ahead of print].
19. Wilson AA, Garcia A, Chestakova A, Kung HF, Houle S. A rapid one-step radiosynthesis of the beta-amyloid imaging radiotracer N-methyl-[^{11}C]2-(4′-methylaminophenyl)-6-hydroxybenzothiazole ([^{11}C]-6-OH-BTA-1). *J Labelled Comp Radiopharm.* 2004;47:679–682.

20. Klok RP, Klein PJ, van Berckel BN, Tolboom N, Lammertsma AA, Windhorst AD. Synthesis of 2-(1,1-dicyanopropen-2-yl)-6-(2-[^{18}F]-fluoroethyl)-methylamino-naphthalene ([^{18}F]FDDNP). *Appl Radiat Isot.* 2008;66:203–207.
21. Maes F, Collignon A, Vandermeulen D, Marchal G, Suetens P. Multimodality image registration by maximization of mutual information. *IEEE Trans Med Imaging.* 1997;16:187–198.
22. Svarer C, Madsen K, Hasselbalch SG, et al. MR-based automatic delineation of volumes of interest in human brain PET images using probability maps. *Neuroimage.* 2005;24:969–979.
23. Wu Y, Carson RE. Noise reduction in the simplified reference tissue model for neuroreceptor functional imaging. *J Cereb Blood Flow Metab.* 2002;22:1440–1452.
24. Yaqub M, Tolboom N, Boellaard R, et al. Simplified parametric methods for [^{11}C]PIB studies. *Neuroimage.* 2008;42:76–86.
25. Yaqub M, Boellaard R, van Berckel BN, et al. Evaluation of tracer kinetic models for analysis of [^{18}F]FDDNP studies. *Mol Imaging Biol.* April 2, 2009 [Epub ahead of print].
26. Innis RB, Cunningham VJ, Delforge J, et al. Consensus nomenclature for in vivo imaging of reversibly binding radioligands. *J Cereb Blood Flow Metab.* 2007;27:1533–1539.
27. Yamaguchi H, Hirai S, Morimatsu M, Shoji M, Nakazato Y. Diffuse type of senile plaques in the cerebellum of Alzheimer-type dementia demonstrated by beta protein immunostain. *Acta Neuropathol.* 1989;77:314–319.
28. Joachim CL, Morris JH, Selkoe DJ. Diffuse senile plaques occur commonly in the cerebellum in Alzheimer's disease. *Am J Pathol.* 1989;135:309–319.
29. Bouwman FH, van der Flier WM, Schoonenboom NS, et al. Longitudinal changes of CSF biomarkers in memory clinic patients. *Neurology.* 2007;69:1006–1011.
30. Thompson PW, Ye L, Morgenstern JL, et al. Interaction of the amyloid imaging tracer FDDNP with hallmark Alzheimer's disease pathologies. *J Neurochem.* 2009;109:623–630.
31. de Leon MJ, Convit A, George AE, et al. In vivo structural studies of the hippocampus in normal aging and in incipient Alzheimer's disease. *Ann N Y Acad Sci.* 1996;777:1–13.
32. Meltzer CC, Leal JP, Mayberg HS, Wagner HN Jr, Frost JJ. Correction of PET data for partial volume effects in human cerebral cortex by MR imaging. *J Comput Assist Tomogr.* 1990;14:561–570.
33. Kloet RW, van Berckel BNM, Pauwels PJW, et al. Effects of MR scanner type, scanning sequence and segmentation algorithm on MR-based partial volume corrections of [^{11}C](*R*)-PK11195 studies [abstract]. *Neuroimage.* 2006;31(suppl 2):T83.

JNM The Journal of NUCLEAR MEDICINE

Relationship of Cerebrospinal Fluid Markers to ^{11}C-PiB and ^{18}F-FDDNP Binding

Nelleke Tolboom, Wiesje M. van der Flier, Maqsood Yaqub, Ronald Boellaard, Nicolaas A. Verwey, Marinus A. Blankenstein, Albert D. Windhorst, Philip Scheltens, Adriaan A. Lammertsma and Bart N.M. van Berckel

J Nucl Med. 2009;50:1464-1470.
Published online: August 18, 2009.
Doi: 10.2967/jnumed.109.064360

The Journal of Nuclear Medicine is published monthly.
SNMMI | Society of Nuclear Medicine and Molecular Imaging
1850 Samuel Morse Drive, Reston, VA 20190.
(Print ISSN: 0161-5505, Online ISSN: 2159-662X)

SNMMI SOCIETY OF NUCLEAR MEDICINE AND MOLECULAR IMAGING